

Initial-Final-Interference and Initial-State-Radiation Effects for Z/γ^* Drell-Yan Observables using $\mathcal{K}\mathcal{K}MC$ -hh

S. Jadach^a, B.F.L. Ward^b, Z. Was^a, S.A. Yost^c

^aInstitute of Nuclear Physics Polish Academy of Sciences, Cracow, PL

^bBaylor University, Waco, TX, USA

^cThe Citadel, Charleston, SC, USA

Abstract

Continuing with our investigations of the expected sizes of multiple photon radiative effects in heavy gauge boson production with decay to charged lepton pairs in the context of the precision physics of the LHC, using $\mathcal{K}\mathcal{K}MC$ -hh 4.22 we consider IFI (initial-final interference) and ISR (initial-state radiation) effects for specific Z/γ^* Drell-Yan observables measured by the ATLAS and CMS Collaborations. With this version of $\mathcal{K}\mathcal{K}MC$ -hh, we have coherent exclusive exponentiation (CEEX) electroweak (EW) exact $O(\alpha^2 L)$ corrections in a hadronic MC and control over the corresponding EW initial-final interference (IFI) effects as well, where the big log L is $\ln \frac{Q^2}{m^2}$ when m is the respective mass of the radiating charged particle which undergoes the momentum transfer Q . Specifically, we illustrate the interplay between cuts of the type used in the measurement of A_{FB} and A_4 at the LHC and the sizes of the expected responses of the attendant higher order corrections. We find that there are per cent to per mille level effects in the initial-state radiation, fractional per mille level effects in the IFI and per mille level effects in the over-all $O(\alpha^2 L)$ corrections that any treatment of EW corrections at the per mille level should consider. Our results are applicable to current LHC experimental data analyses.

1 Introduction

The large data samples at 7TeV and the even larger data samples at 8TeV and 13TeV have ushered in the era of precision QCD \otimes EW physics for the LHC experiments for processes such as single heavy gauge boson production with decay to lepton pairs. As examples, the ATLAS Collaboration has recently used 8 TeV data samples to measure the Drell-Yan angular coefficients [1] A_0, \dots, A_7 as a prelude to a precision measurement of $\sin^2\theta_W$. These measurements have been followed by their use of their 7 TeV data samples to measure the mass of the W boson with the result Ref. [2]:

$$M_W = 80370 \pm 7(\text{stat.}) \pm 11(\text{exp. syst.}) \pm 14(\text{mod. syst.})\text{MeV} = 80370 \pm 19\text{MeV},$$

where the first uncertainty is statistical, the second is the experimental systematic uncertainty, and the third is the physics-modeling systematic uncertainty. As one of the most precise single measurements of M_W [3] the result bodes well, given the remaining data samples that have yet to be analyzed, for a new level of precision in the observable M_W as well as other EW observables in LHC physics. High precision in measurements of lepton directions in detectors of hadron colliders is the essential feature, see eg. Ref. [4].

From the error budget the ATLAS measurement of M_W we see the importance of the modeling systematic error as it is the largest contribution with a value of 14 MeV. Given that the corresponding statistical error will be reduced by a factor of ~ 4 when all of the available data are analyzed, it is necessary to reduce the large modelling error in kind as much as possible. We note that, in the measurement of M_W by the ATLAS Collaboration [2] the W production and decay systematics are estimated by comparison with the analogous systematics for the Z/γ^* production and decays. The latter systematics are impacted by the uncertainty on the corresponding EW corrections.

We have discussed the sizes of the various relevant EW corrections on the observables such as the Z/γ^* p_T , the lepton p_T and di-lepton invariant mass in Ref. [5]. What we have found can be illustrated by a comparison of the results, with ATLAS cuts, from $\mathcal{K}\mathcal{K}\text{MC-hh}$ for the lepton p_T spectrum in Fig. 1 in [5] with the ATLAS ratio plot between their data and the best theory predictions which they employ as presented in their Fig. 15 in Ref. [2]. If we look at the effect of the ISR on this spectrum as predicted by $\mathcal{K}\mathcal{K}\text{MC-hh}$ we see that it agrees with the fact that the ATLAS data are about 1-2% above the theory which they use at the low p_T end of the respective plot and a similar amount below the theory at the high end of that plot. This is expected because the theory used by ATLAS, which features the QED ISR from the respective Pythia [6] shower, does not have the full effect of the ISR from the transverse degrees of freedom for the radiation featured in the respective $\mathcal{K}\mathcal{K}\text{MC-hh}$ predictions.

Similarly, in the ATLAS and CMS measurements of the angular coefficients [1, 7], the systematics of the respective modelling errors are impacted by the uncertainty on the respective EW corrections. In what follows, we will explore to what extent the various aspects of the EW corrections interplay with the ATLAS-type cuts and the method of application of the corrections.

A key issue in this interplay is the role of phase space competition between photons and gluons in the multiple photon and multiple gluon processes under study here. Specifically, in Ref. [8] in the context of FSR (final-state radiation) at LEP, it was shown that the competition

between parton shower gluons and parton shower photons led to considerable reduction in the available phase space for photons when the QED and QCD showers were interleaved relative to the situation in which the two showers are not interleaved. A natural question to ask is whether we have to take such a reduction into account in our calculations with $\mathcal{K}\mathcal{KMC}$ -hh for the respective Z/γ^* observables which we study? The key point in the results in Ref. [8] is that in the infrared regime, with energy fraction $\lesssim 0.1$, there is essentially no effect of phase space competition between the interleaved gluon and photon showers. This is important because in $\mathcal{K}\mathcal{KMC}$ -hh we resum the infrared regime to all orders in α in the presence of hard photon residuals. The hard photon residuals are separated in space-time from the gluon shower quanta in the standard inside-out cascade, so that there is also no phase space competition between the hard photon residuals and the shower gluons. What we can have is a phase space competition between the hard photon residuals and the hard gluons in our processes, where the first such effects occur at $O(\alpha\alpha_s)$. The size of such hard non-factorizable two-loop effects has been studied in Ref. [9, 10] and it is expected to be below the level of precision in the studies we present here.

We should also call attention to the studies in Refs. [11, 12, 13, 14, 15] and in Ref. [16] on the expected sizes of the EW corrections in LHC observables. We the detailed relationship between our $\mathcal{K}\mathcal{KMC}$ -hh results and those in these latter references will be addressed elsewhere [17]¹. For neutral current Drell-Yan processes, Herwig [19], Pythia [6, 20], Herwig++ [21] and Sherpa [22] have featured QED radiative effects in the context of parton showers: the leading-log QED shower is implemented in Herwig, Herwig++, Pythia and Sherpa and final-state YFS [23] exponentiated radiation for decays is implemented in Herwig++ and in Sherpa, where in Sherpa the NLO EW and QED NNLO exact YFS residuals (see Ref. [23] for their definition) have been realized [24] in this context. In Refs. [25, 26, 27], Sherpa, Recola and OpenLoops authors have also made available exact $O(\alpha)$ EW corrections and exact NLO QCD corrections to such Drell-Yan processes as an option with parton showers. In the Powheg framework, the corresponding exact $O(\alpha)$ EW corrections and exact NLO QCD corrections are realized as presented in Ref. [28]. We additionally observe that SANC [29] features NLO EW and NLO QCD corrections to neutral current Drell-Yan processes and that FEWZ [30] realizes the exact $O(\alpha)$ EW corrections along with its exact NNLO QCD corrections to such processes. We would again note the exact $O(\alpha\alpha_s)$ non-factorizable corrections to the neutral current Drell-Yan process already referenced in Refs. [9, 10], which are available, along with the NLO QCD and NLO EW corrections, in the MC integrator program RADY. In the connection of mixed $O(\alpha\alpha_s)$ corrections, we finally note the studies in Refs. [31, 32] for on-shell Z production.

The paper is organized as follows. In the next section we give a brief review of the physics in the $\mathcal{K}\mathcal{KMC}$ -hh MC, as it is still not a generally familiar. In Section 3 we illustrate the effect of the EW corrections in $\mathcal{K}\mathcal{KMC}$ -hh in the context of the acceptance used by ATLAS in their studies of the angular coefficient A_4 and A_{FB} in single Z/γ^* events with decays to lepton pairs in Ref. [1]. In this section, we make contact with the studies in Ref. [16]. In Section 4, we summarize our findings.

¹This relationship is part of the ongoing studies in the CERN LPCC EW Precision Subgroup Meetings: <https://lpcc.web.cern.ch/electroweak-precision-measurements-lhc-wg> [18].

2 The Physics in $\mathcal{K}\mathcal{K}\text{MC-hh}$

In $\mathcal{K}\mathcal{K}\text{MC-hh}$ we combine the exact amplitude-based CEEX/EEX YFS MC approach to EW higher order corrections pioneered in Refs. [33, 34, 35, 36] and the QCD parton shower hadron MC approach pioneered in Refs. [37, 19]. Here, EEX denotes exclusive exponentiation as originally formulated by Yennie, Frautschi and Suura (YFS) in Ref. [23]. In the discussion which follows, we will use the Herwig6.5 [19] MC for the parton shower realization although the use of any parton shower MC which accepts LHE [38] input is allowed in $\mathcal{K}\mathcal{K}\text{MC-hh}$ studies. We now give a brief review of the physics in $\mathcal{K}\mathcal{K}\text{MC-hh}$.

Since it is still not generally used, we recall the master formula for the CEEX realization of the higher corrections to the SM [39, 40, 41, 42] EW theory. For clarity, we note that the CEEX realization is amplitude level coherent exclusive exponentiation whereas the EEX realization is exclusive exponentiation at the squared amplitude level. For the purpose of illustration, let us consider the prototypical process $q\bar{q} \rightarrow \ell\bar{\ell} + n\gamma$, $q = u, d, s, c, b, t$, $\ell = e, \mu, \tau, \nu_e, \nu_\mu, \nu_\tau$. For this process, we have the cross section formula

$$\sigma = \frac{1}{\text{flux}} \sum_{n=0}^{\infty} \int d\text{LIPS}_{n+2} \rho_A^{(n)}(\{p\}, \{k\}), \quad (1)$$

where LIPS_{n+2} denotes Lorentz-invariant phase-space for $n+2$ particles, $A = \text{CEEX}, \text{EEX}$, the incoming and outgoing fermion momenta are abbreviated as $\{p\}$ and the n photon momenta are denoted by $\{k\}$. Thanks to use of conformal symmetry, full $2+n$ body phase space is covered without any approximations. The respective algorithm's details are covered in Ref. [34]. Specifically, we have from Refs. [35, 34, 43] that

$$\rho_{\text{CEEX}}^{(n)}(\{p\}, \{k\}) = \frac{1}{n!} e^{Y(\Omega; \{p\})} \bar{\Theta}(\Omega) \frac{1}{4} \sum_{\text{helicities } \{\lambda\}, \{\mu\}} \left| \mathcal{M} \left(\begin{matrix} \{p\} \{k\} \\ \{\lambda\} \{\mu\} \end{matrix} \right) \right|^2. \quad (2)$$

(For the corresponding formula for the $A = \text{EEX}$ case we refer the reader to Refs. [35, 34].) Here, $Y(\Omega; \{p\})$ is the YFS infrared exponent. The respective infrared integration limits are specified by the region Ω and its characteristic function $\Theta(\Omega, k)$ for a photon of energy k , with $\bar{\Theta}(\Omega; k) = 1 - \Theta(\Omega, k)$ and

$$\bar{\Theta}(\Omega) = \prod_{i=1}^n \bar{\Theta}(\Omega, k_i).$$

The definitions of the latter functions as well as the CEEX amplitudes $\{\mathcal{M}\}$ are given in Refs. [34, 35, 36]. $\mathcal{K}\mathcal{K}\text{MC-hh}$ obtains from $\mathcal{K}\mathcal{K}\text{MC}$ 4.22 the exact $O(\alpha)$ EW corrections implemented using the DIZET 6.21 EW library from the semi-analytical program ZFITTER [44, 45]. The respective implementation is described in Ref. [35] so that we do not repeat it here. In $\mathcal{K}\mathcal{K}\text{MC-hh}$, the CEEX amplitudes $\{\mathcal{M}\}$ in (2) are exact in $O(\alpha^2 L^2, \alpha^2 L)$ in the sense that all terms in the respective cross section at orders $O(\alpha^0)$, $O(\alpha)$, $O(\alpha L)$, $O(\alpha^2 L)$, and $O(\alpha^2 L^2)$ are all included in our result for that cross section. Here the big log is $L = \ln \frac{Q^2}{m^2}$ where Q is the respective hard 4-momentum transfer. In our case, the light quark masses and the charged lepton masses will determine m , depending on the specific process under consideration. We

follow Ref. [46] and use the current quark masses [47] $m_u = 2.2\text{MeV}$, $m_d = 4.7\text{MeV}$, $m_s = 0.150\text{GeV}$, $m_c = 1.2\text{GeV}$, $m_b = 4.6\text{GeV}$, and $m_t = 173.5\text{GeV}$.

The realization of the parton shower MC approach proceeds via the standard Drell-Yan formula for the process $pp \rightarrow Z/\gamma^* + X \rightarrow \ell\bar{\ell} + X'$, $\ell = e^-, \mu^-$:

$$\sigma_{\text{DY}} = \int dx_1 dx_2 \sum_i f_i(x_1) f_{\bar{i}}(x_2) \sigma_{\text{DY},i\bar{i}}(Q^2) \delta(Q^2 - x_1 x_2 s), \quad (3)$$

where the subprocess cross section for the i -th $q\bar{q}$ annihilation with $\hat{s} = Q^2$ when the pp cms energy squared is s is denoted in a conventional notation for parton densities $\{f_j\}$. Here, $\sigma_{\text{DY},i\bar{i}}(Q^2)$ is given by the right-hand-side of Eq. 1, realized by Monte Carlo methods as explained in Refs. [36, 43]. $\mathcal{K}\mathcal{K}\text{MC-hh}$ receives multiple gluon radiation, for a given QCD parton shower MC, via the backward evolution [37] for the densities as specified in (3). This backward evolution then also affords $\mathcal{K}\mathcal{K}\text{MC-hh}$ the hadronization for the attendant shower. While we use here the Herwig6.5 shower MC for this phase of the event generation, we note, again, that, as the Les Houches Accord format is also available for the hard processes generated in $\mathcal{K}\mathcal{K}\text{MC-hh}$ before the shower, all shower MC's which use that format can be used for the shower/hadronization part of the simulation.

3 CEEEX Exact $O(\alpha^2 L)$ EW IFI and ISR Effects from $\mathcal{K}\mathcal{K}\text{MC-hh}$ for the ATLAS Acceptance for Z/γ^* Drell-Yan Observables

As we have noted, in both the ATLAS and the CMS Collaborations measurements of the Z/γ^* decay angular coefficients [1, 7], the systematics of the respective modelling errors are impacted by the uncertainty on the respective EW corrections. In this section we use the Z/γ^* cuts that are typical of the systematics studies done by ATLAS in their angular coefficients and m_W analysis, as motivated by our participation in the CERN Precision Studies Subgroup of the LPCC EWWG³, to illustrate the size of the new higher order EW effects in $\mathcal{K}\mathcal{K}\text{MC-hh}$ in the context of those cuts for the angular coefficients and related observables.

The ATLAS-type cuts on the Z/γ^* production and decay to lepton pairs, as employed in Ref. [1, 2], which we use are as follows:

$$60 \text{ GeV} < M_{\ell\ell} < 116 \text{ GeV}, \quad P_T^{\ell\ell} < 30 \text{ GeV},$$

where both members of the decay lepton pair satisfy

$$P_T^\ell > 25 \text{ GeV}, \quad |\eta_\ell| < 2.5.$$

²See Ref. [5] for a discussion of the uncertainty of our results due to realistic uncertainties on our values of the current quark masses.

³<https://lpc.web.cern.ch/electroweak-precision-measurements-lhc-wg> [18] - note that several of the authors of the purely collinear QED PDF approaches presented in Ref. [16] are involved in these studies.

Here, we have defined $M_{\ell\ell}$ as the lepton pair invariant mass, $P_T^{\ell\ell}$ as the transverse momentum of the lepton pair, P_T^ℓ as the transverse momentum of the lepton or anti-lepton ℓ , and η_ℓ as the pseudorapidity of the lepton or anti-lepton ℓ .

We start with the basic kinematics for the observables which we study, as it is shown in Fig. 1. We work in the Collins-Soper(CS) frame for the outgoing lepton pair with the Collins-

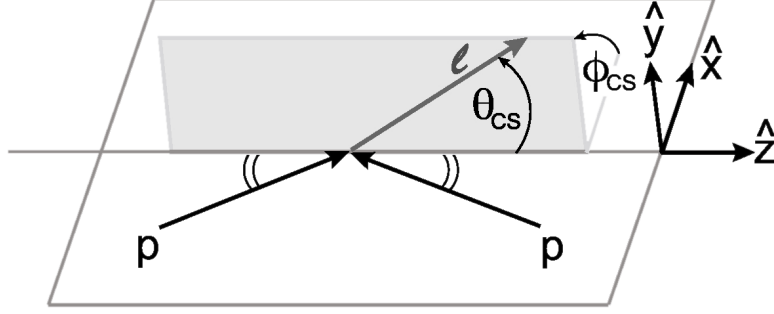


Figure 1: Kinematics of the lepton decay angles in the Collins-Soper frame [1, 48]. The Collins-Soper angle is given by $\cos\theta_{CS} = \text{sgn}(P_{\ell\ell}^z) \frac{p_{\ell_1}^+ p_{\ell_2}^- - p_{\ell_1}^- p_{\ell_2}^+}{M_{\ell\ell} \sqrt{M_{\ell\ell}^2 + P_{T\ell\ell}^2}}$ with $p^\pm = p^0 \pm p^z$. $P_{\ell\ell} = p_{\ell_1} + p_{\ell_2}$, where $\ell_1 = \ell^- \equiv \ell$ in the illustration and $\ell_2 = \ell^+ \equiv \bar{\ell}$. The laboratory z-axis may taken as that given in Ref. [49].

Soper [48] polar and azimuthal angles θ_{CS} , ϕ_{CS} as shown in Fig. 1. Since we are interested in the systematics associated with the extraction of $\sin^2\theta_W$ from the respective data, we will focus on the angular distribution for θ_{CS} and the observables A_4 and A_{FB} , which we define as

$$A_4 = \frac{4}{\sigma} \int \cos\theta_{CS} d\sigma = 4 \langle \cos\theta_{CS} \rangle$$

$$A_{FB} = \frac{1}{\sigma} \int \text{sgn}(\cos\theta_{CS}) d\sigma = \langle \text{sgn}(\cos\theta_{CS}) \rangle$$

where we follow the notation of Ref. [50] for the angular coefficients A_i , $i = 0, \dots, 7$ in the respective differential cross section $d\sigma(\theta_{CS}, \phi_{CS})$ for the lepton in Fig. 1⁴.

As we have shown in Ref. [5] QED ISR (initial-state radiation) enters the angular distributions at the level of several per mille and cannot be neglected. In what follows, we compare our exact $O(\alpha^2 L)$ CEEX treatment of these effects in $\mathcal{K}\mathcal{K}\text{MC-hh}$ with their treatment in the QED-pdf approach as it is realized with the LuxQED [51] formulation as realized in the NNPDF 3.1 NLO ($\alpha_s(M_Z) = 0.118$) set [52]. We expect that the two approaches should agree when effects are not sensitive to the photon transverse momentum $p_{\gamma,T}$.

⁴Consideration of more radiative effects than those discussed explicitly in Ref. [50] will lead, in general, to the introduction of coefficients beyond those in Ref. [50] for higher ℓ spherical harmonics Y_ℓ^m ; as these are orthogonal to Y_1^0 , our formula for A_4 is unaffected but the relationship between A_4 and A_{FB} is affected as for example Y_3^0 has a forward-backward asymmetry.

Specifically, we turn first to comparisons featuring unshowered results using $\mathcal{K}\mathcal{KMC}$ -hh in which we have a sample of 5.7×10^9 muon-pair events⁵ at 8 TeV. In the discussion of our results, "uncut/without cuts" means that no additional cuts beyond the muon-pair mass cut $60 \text{ GeV} < M_{\ell\ell} < 116$ are made whereas "cut/with cuts" means that the additional cuts $P_T^\ell > 25 \text{ GeV}$, $|\eta_\ell| < 2.5$ are made on both members of the muon pair in conjunction with the cut $P_T^{\ell\ell} < 30$. Under these circumstances, we present four levels of photonic corrections:

1. Final-state radiation(FSR) using $\mathcal{K}\mathcal{KMC}$ -hh with non-QED NNPDF3.1 NLO
2. FSR + initial-state radiation (ISR) using $\mathcal{K}\mathcal{KMC}$ -hh with non-QED NNPDF3.1 NLO
3. FSR + ISR + initial-final interference (IFI) radiative effects using $\mathcal{K}\mathcal{KMC}$ -hh with non-QED NNPDF3.1 NLO (the best $\mathcal{K}\mathcal{KMC}$ -hh result)
4. FSR + LuxQED using $\mathcal{K}\mathcal{KMC}$ -hh with QED NNPDF3.1 NLO.

The $\mathcal{K}\mathcal{KMC}$ -hh photonic corrections are calculated using CEEX exponentiation with exact $O(\alpha^2 L)$ residuals.

We present in Table 1 results for the uncut and cut cross sections and for the A_{FB} and A_4 observables for the four levels of photonic corrections as described. For the uncut and cut cross

Table 1: Numerical Results

	No ISR	LuxQED	$\mathcal{K}\mathcal{KMC}$ -hh ISR	%(ISR-no ISR)	With IFI	%(IFI - no IFI)
Uncut σ (pb)	939.86(1)	944.04(1)	944.99(2)	0.54597(2)	944.91(2)	-0.0089(4)
Cut σ (pb)	439.10(1)	440.93(1)	442.36(1)	0.74223(3)	442.33(1)	-0.0070(5)
	No ISR	LuxQED	$\mathcal{K}\mathcal{KMC}$ -hh ISR	ISR- no ISR	With IFI	IFI - no IFI
A_{FB}	0.01125(2)	0.01145(2)	0.01129(2)	$(3.9 \pm 2.8) \times 10^{-5}$	0.01132(2)	$(2.9 \pm 1.1) \times 10^{-5}$
A_4	0.06102(3)	0.06131(3)	0.06057(3)	$-(4.4 \pm 0.5) \times 10^{-5}$	0.06102(3)	$(4.5 \pm 0.3) \times 10^{-5}$

sections, we see that $\mathcal{K}\mathcal{KMC}$ -hh shows an ISR effect of a fraction greater than half of a percent. LuxQED shows a slightly smaller effect, about 0.4% for each cross section. $\mathcal{K}\mathcal{KMC}$ -hh shows an IFI effect below 0.1%. On the the angular coefficients the ISR and IFI effects are both on the order of 10^{-5} in $\mathcal{K}\mathcal{KMC}$ -hh. LuxQED gives a somewhat bigger ISR effect in this case, on the order of 10^{-4} .

We turn next to the ISR contributions to the distribution of the cosine of the CS angle. This is shown in Fig. 2. We see that ISR enters at the per mille level. It must be taken into account in precision studies of this process⁶.

To see how the effects in Fig. 2 affect the angular coefficients, we turn next to results for A_{FB}

⁵In this paper we focus on muon pairs in the Z/γ^* decays so that we avoid the issues of calorimetry for e^+e^- pairs and of tau decays in $\tau^+\tau^-$ pairs. The latter two scenarios will be taken up elsewhere [17]. Note that it is known that IFI is roughly the same for both bare and dressed FSR because IFI comes mainly from photons in the middle of the angular range between IS and FS charges. Since the data in Ref. [1] are at the Born Z level to facilitate combination of electron and muon data, our treatment of bare muons allows one to see the relative sizes of the ISR and IFI effects we calculate compared to the FSR used to arrive at Born Z results.

⁶As in LEP we expect the experimental statistical errors in angular distribution measurements to reflect the size of the experimental errors and we need that the theory errors stay at or below 1/3 of the experimental errors so that the former do not significantly affect the latter. As one can see, for example, from Table 9 in Ref. [1] the experimental statistical error on A_4 in the 5 - 8 GeV p_T bin is 1 per mille based on 20.3 fb^{-1} of data. Since there remain 143.6 fb^{-1} of data to be analyzed, we have a budget for the theory error at or below 1 per mille/ $(3 \times \sqrt{163.9/20.3}) \cong 0.00012$. All effects that are at or above this level have to be taken into account.

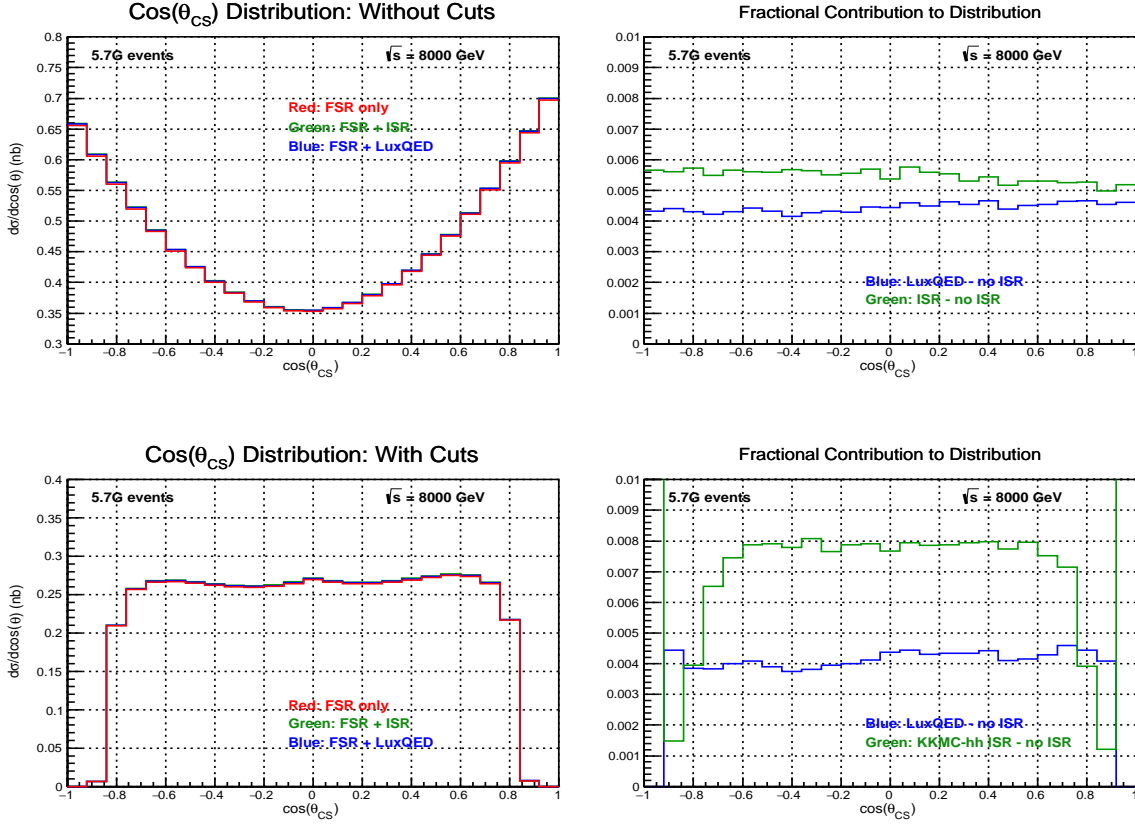


Figure 2: ISR contribution to the CS angle distribution: the two top plots are without lepton cuts (used for A_4), the two bottom plots are with lepton cuts (used for A_{FB}). LuxQED ISR + FSR is in blue(dark shade), $\mathcal{K}\mathcal{K}MC$ -hh ISR+ FSR is in green (light shade), and FSR only, the baseline here, is in red (medium dark shade). In the two plots on the right, the respective FSR only plot is subtracted from the LuxQED ISR + FSR (blue) and $\mathcal{K}\mathcal{K}MC$ -hh ISR + FSR (green) plots.

as shown in Fig. 3. The ISR contribution to A_{FB} is typically on the per mille level. For most $M_{\ell\ell}$ of interest, LuxQED and $\mathcal{K}\mathcal{K}MC$ -hh produce very similar ISR effects. Integrating over $M_{\ell\ell}$ and binning in $|Y_{\ell\ell}|$, both LuxQED and $\mathcal{K}\mathcal{K}MC$ -hh give ISR contributions on the order of 10^{-4} , with the $\mathcal{K}\mathcal{K}MC$ -hh correction smaller at low rapidities. It should be taken into account in precision studies of this process.

Continuing in this way, we show our results for the angular coefficient A_4 in Fig. 4. The ISR contribution to A_4 is typically on the order of 10^{-3} , but differs in detail between LuxQED and $\mathcal{K}\mathcal{K}MC$ -hh. When integrated over $M_{\ell\ell}$ and binned in $|Y_{\ell\ell}|$, the ISR contribution is a little smaller, and of order 10^{-4} for $\mathcal{K}\mathcal{K}MC$ -hh at low rapidities. It should be taken into account in precision studies of this process.

We turn next to the initial-state-final-state interference (IFI) effects. We point-out that, due to IFI, it is not possible to separate unambiguously photon radiation into ISR and FSR. This complicates the interpretation of A_{FB} and A_4 unless IFI can be shown to be sufficiently small. Exponentiation at the amplitude level (CEEX), instead of the cross section level (EEX) facil-

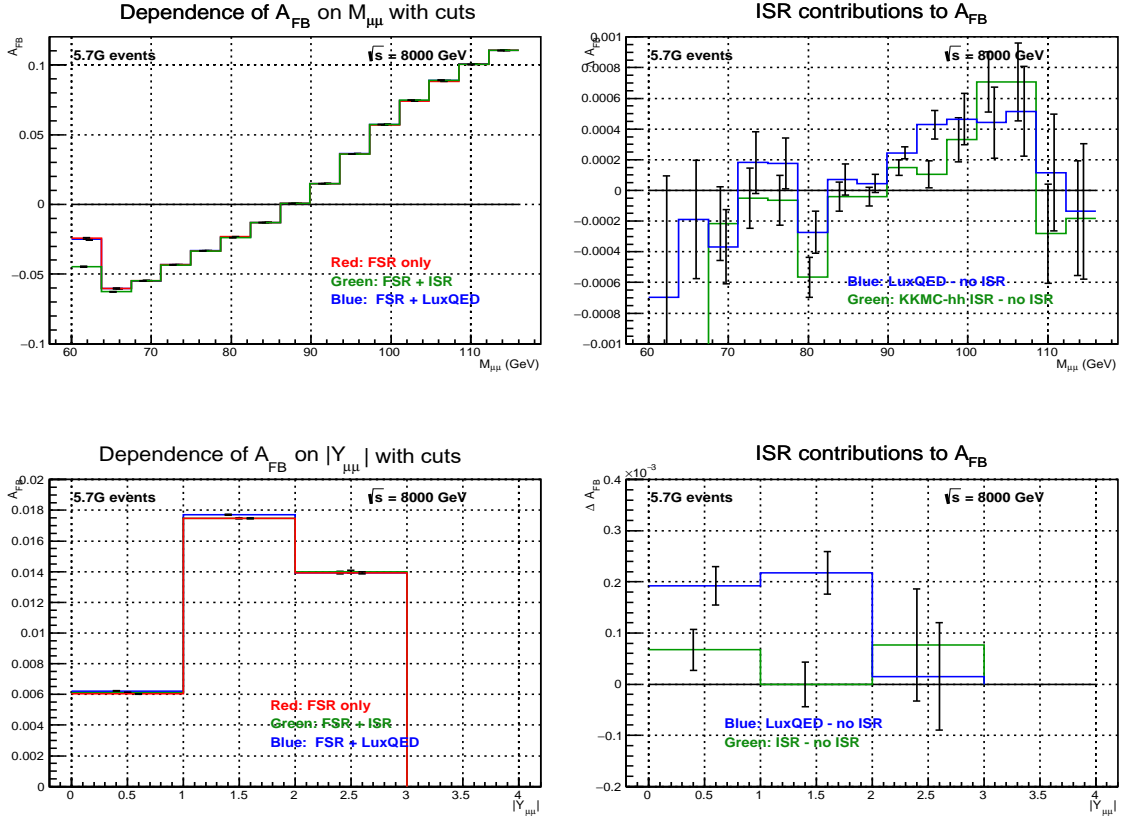


Figure 3: ISR contributions to A_{FB} with lepton cuts. Results are shown for FSR only, LuxQED ISR + FSR and $\mathcal{K}\mathcal{KMC}$ -hh ISR + FSR. The color scheme for the plots is the same as that in Fig. 2. The plots on the right show the respective differences between the FSR only plot and the plots with ISR + FSR. Results are plotted as functions of $M_{\ell\ell}$ (top plots) and as functions of $|Y_{\ell\ell}|$.

itates the calculation of interference effects. This is one of the primary reasons CEEEX was introduced, when effects at this level became relevant at LEP. IFI is implemented in CEEEX by dividing the generated photons into partitions of ISR and FSR, and summing over all such partitions. In the following, we compare $\mathcal{K}\mathcal{KMC}$ -hh results with IFI turned on or off. The effect on angular variables is shown in terms of $M_{\ell\ell}$ and $|Y_{\ell\ell}|$ bins.

We study first the effects of IFI on the distribution of the cosine of the CS angle with and without lepton cuts in Fig. 5. Both with and without the lepton cuts, there are IFI effects at the 10^{-4} level, but with very different dependencies on $\cos\theta_{CS}$. To be on the safe side, precision studies should take these effects into account.

Focusing next of the angular observables, we show the IFI effects on A_{FB} in Fig. 6. The IFI contribution to A_{FB} is generally less than 10^{-3} . When integrated over $M_{\ell\ell}$, the IFI contribution is typically less than 10^{-4} , and much less for small rapidities. In general, precision studies should take this contribution into account.

Similarly, we show the IFI effects on A_4 in Fig. 7. The IFI contribution to A_4 is generally less

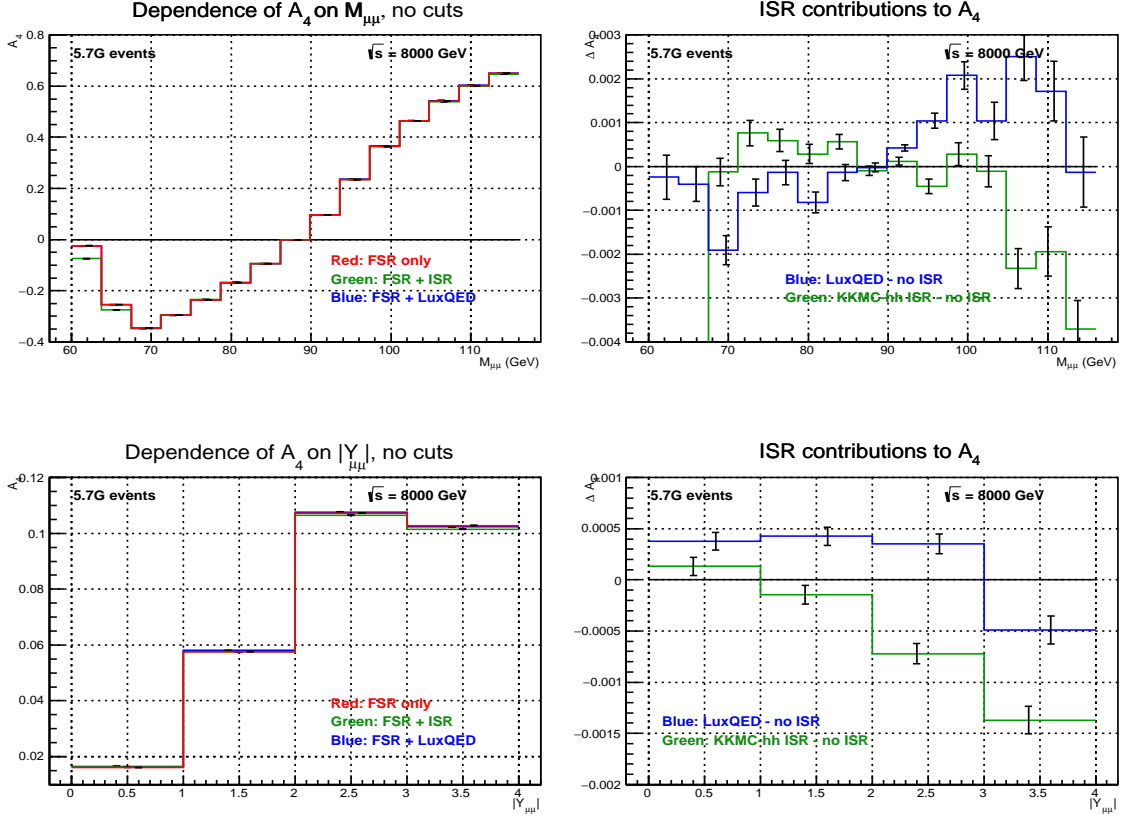


Figure 4: ISR contributions to A_4 without lepton cuts, to remain consistent with the formula we use for it. Results are shown for FSR only, LuxQED ISR + FSR and $\mathcal{K}\mathcal{K}\text{MC-hh}$ ISR + FSR. The color scheme for the plots is the same as that in Fig. 2. The plots on the right show the respective differences between the FSR only plot and the plots with ISR + FSR. Results are plotted as functions of $M_{\ell\ell}$ (top plots) and as functions of $|Y_{\ell\ell}|$ (bottom plots).

than 10^{-2} but depends on $M_{\ell\ell}$. When integrated over $M_{\ell\ell}$, the IFI contribution is generally less than 10^{-3} , and very small for some rapidities. Precision studies should take this contribution into account.

We turn now to the effect of the parton shower on the previous results. We use the built-in Herwig 6.521 [19] shower but we stress that, due to the LHE format in $\mathcal{K}\mathcal{K}\text{MC-hh}$, in principle any shower compatible with that format can be used. In Table 2, we show the numerical effect of the shower on results for the cross section, A_{FB} , and A_4 from $\mathcal{K}\mathcal{K}\text{MC-hh}$ with the ISR on and the non-QED NNPDF 3.1 NLO PDF. The results are determined from a sample of 1.1×10^9 events at 8 TeV. The results are shown for both the cut and uncut cases. For the uncut cases, we see effects at the % level. For the cut cases, we see effects at the 7 - 8 % level. We note that, as the shower does not affect the overall normalization, we expect smaller effects from the shower in the uncut scenarios and larger effects in the cut cases in which the available phase space is much more restricted. Our results support this expectation. Precision studies should take these effects into account.

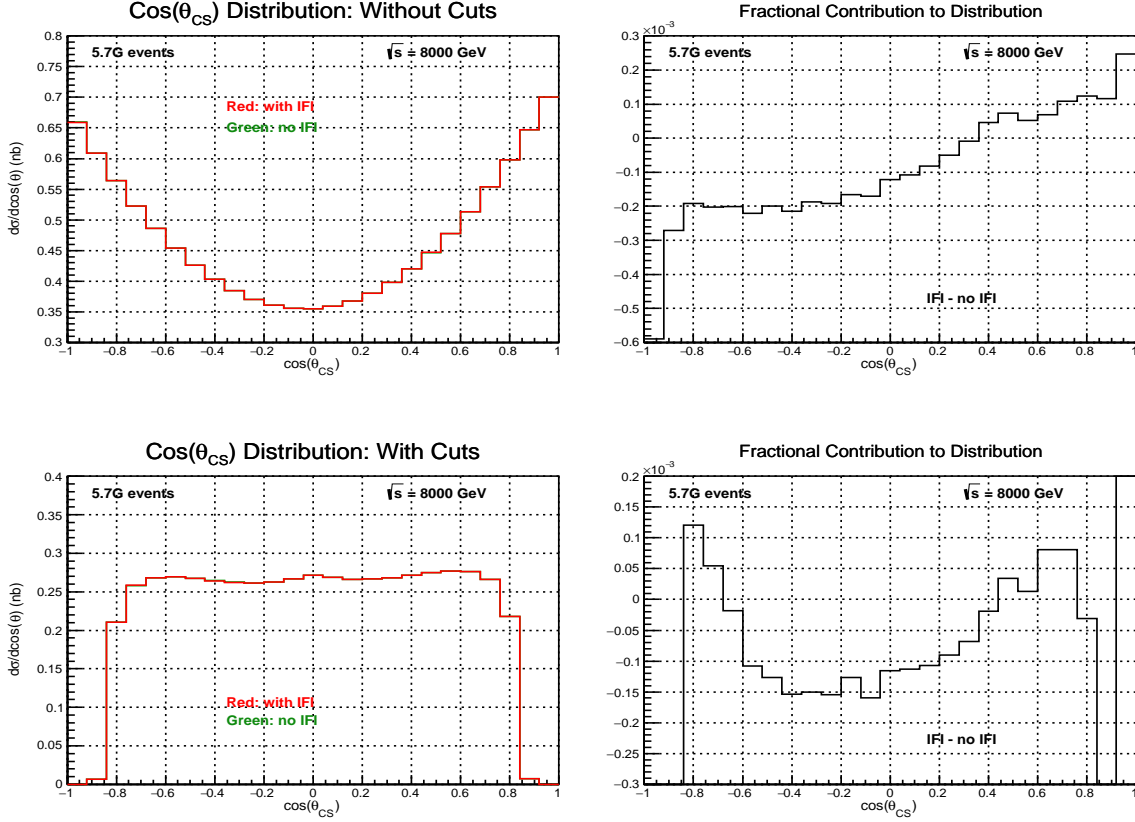


Figure 5: IFI contribution to the distribution of $\cos\theta_{CS}$ without lepton cuts (for A_4) in the top plots and with lepton cuts (for A_{FB}) in the bottom plots. Results are shown for $\mathcal{K}\mathcal{K}MC$ -hh ISR + FSR in red (medium dark shade) and for $\mathcal{K}\mathcal{K}MC$ -hh ISR + FSR+IFI in green (light shade). The plots on the right show the respective fractional IFI contribution to the distributions on the left.

Table 2: Showered Numerical Results: σ , A_{FB} , A_4

	Without Shower	With Shower	% Difference
Uncut σ (pb)	944.91(2)	938.44(4)	-0.684(7)%
Cut σ (pb)	442.33(1)	412.54(3)	-6.7307%
	without Shower	With Shower	Difference
A_{FB}	0.01132(2)	0.01211(5)	0.00109(5)
A_4	0.06102(8)	0.06052(8)	-0.00050(8)

Considering the IFI contributions to the cross section with and without cuts, we show the effects of the shower in Table 3. In each case, the IFI contribution is significantly smaller with the shower on.

The comparisons between the showered and unshowered results for the IFI contributions to A_{FB} and to A_4 are shown in Table 4. The effect of the shower on the IFI contribution is statistically insignificant for A_4 and is barely significant, of order 10^{-5} , for A_{FB} .

We turn next to the effects of the shower on the angular distribution plotted as a function of

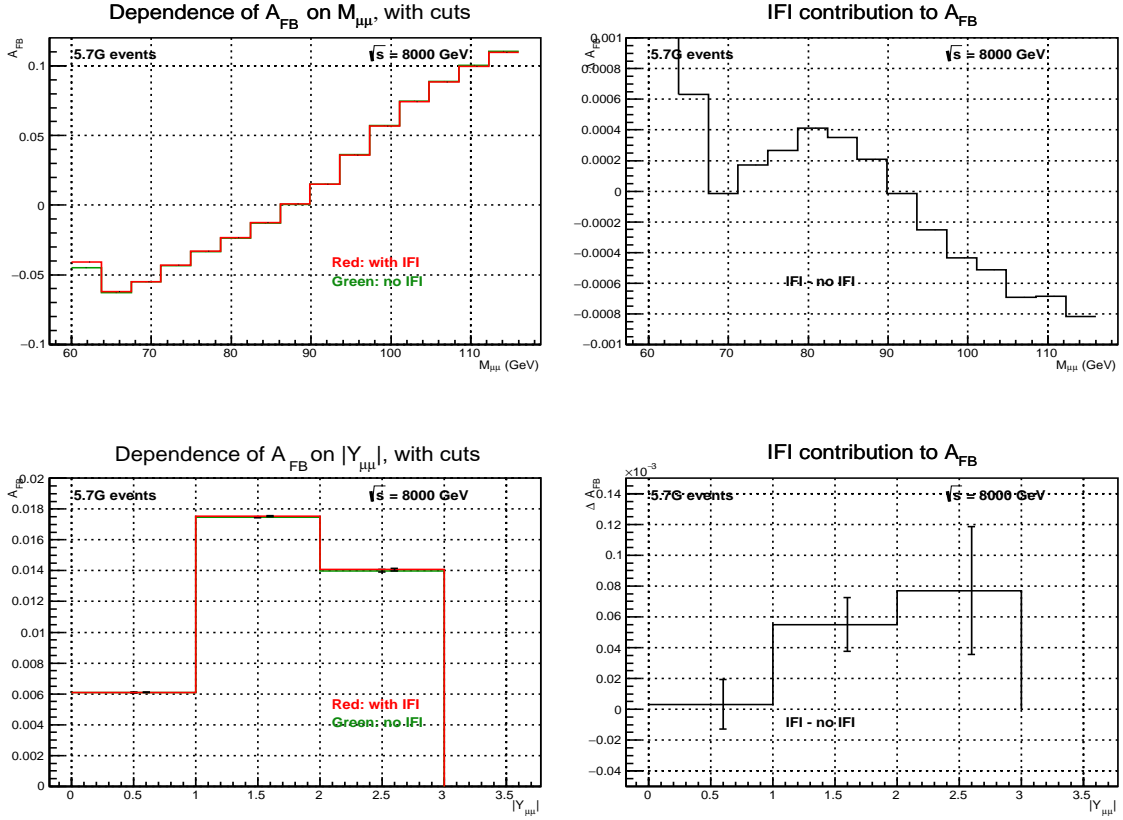


Figure 6: IFI contribution to A_{FB} with lepton cuts. Results are shown for $\mathcal{K}\mathcal{K}MC$ -hh ISR + FSR in red (medium dark shade) and for $\mathcal{K}\mathcal{K}MC$ -hh ISR + FSR+IFI in green (light shade). The plots on the right show the respective IFI contribution to the distributions on the left. Results are plotted as functions of $M_{\ell\ell}$ (top plots) and as functions of $|Y_{\ell\ell}|$ (bottom plots).

$\cos(\theta_{CS})$ which we exhibit in Fig. 8. We see that the shower effects enter at the per cent level without cuts and enter at the 10-20% level with cuts.

In Fig. 9 we show the effect of the shower on the IFI contribution, calculated with $\mathcal{K}\mathcal{K}MC$ -hh, to the uncut and cut CS angle distributions. The IFI effect is angle-dependent and is at the level of a fraction of a per mille and the shower produces an angle-dependent modulation which still leaves the effect at the fractional per mille level.

In Fig. 10 we show the effects of the shower on A_{FB} as a function of $M_{\ell\ell}$ and as a function of $Y_{\ell\ell}$. The effect of the shower on increases for $M_{\ell\ell}$ away from M_Z where A_{FB} is suppressed. The effect of the shower on A_{FB} increases for larger rapidities $Y_{\ell\ell}$. It is well-known that precision studies should take these effects into account.

Similarly, in Fig. 11, we show the shower effects on the IFI contribution to A_{FB} as a function of $M_{\ell\ell}$ and as a function of $Y_{\ell\ell}$. The shower gives a mild modulation of the IFI effect as a function of $M_{\ell\ell}$; for the dependence on $Y_{\ell\ell}$, modulation is within the statistical errors.

In Fig. 12 we show the effects of the shower on A_4 . The effect of the shower on A_4 is small for $M_{\ell\ell} \geq M_Z$. As a function the rapidity, the effect of the shower on A_4 is fairly small except

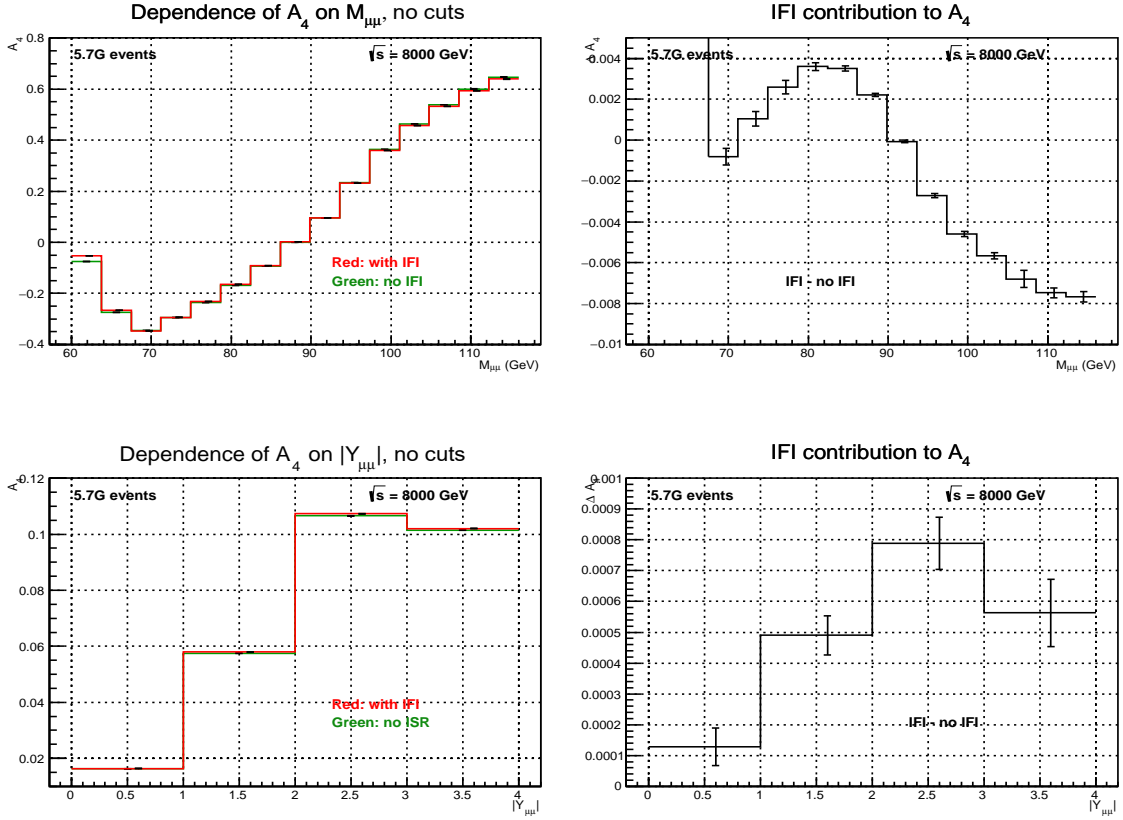


Figure 7: IFI contribution to A_4 without lepton cuts. Results are shown for $\mathcal{K}\mathcal{K}\text{MC-hh ISR} + \text{FSR}$ in red (medium dark shade) and for $\mathcal{K}\mathcal{K}\text{MC-hh ISR} + \text{FSR} + \text{IFI}$ in green (light shade). The plots on the right show the respective IFI contribution to the distributions on the left. Results are plotted as functions of $M_{\ell\ell}$ (top plots) and as functions of $|Y_{\ell\ell}|$ (bottom plots).

for large values of $Y_{\ell\ell}$.

The shower effects on the IFI contribution to A_4 are studied in Fig. 13. There are modulations by the shower of both the distribution in $M_{\ell\ell}$ and the distribution in $Y_{\ell\ell}$. Precision studies should not ignore these effects as it is well-known.

4 Summary

Our results show that ISR typically enters the angular results (A_{FB}, A_4) at the level of several per mille. Both $\mathcal{K}\mathcal{K}\text{MC-hh}$ and QED PDFs give a comparable ISR effect on angular results. The IFI effect is typically one-tenth the ISR effect or less, but this is sensitive to cuts. The parton shower changes the detailed results, but not the general size of the ISR and IFI corrections. A more complete treatment of the respective QCD corrections, accurate to NLO, in the presence of our exact $\mathcal{O}(\alpha^2 L)$ CEEW EW corrections will appear elsewhere [17].

Studies [18] are underway to clarify the role of ISR and IFI in the precision determination

Table 3: Showered Results: IFI Contributions to σ

Uncut σ	No IFI (pb)	With IFI (pb)	% Difference
No Shower	944.99(2)	944.91(2)	-0.0089(4)%
Shower	938.46(4)	938.44(4)	-0.002(1)%
Difference	-0.691(5)%	-0.684(5)%	0.007(1)%
Cut σ	No IFI (pb)	With IFI (pb)	% Difference
No Shower	442.36(1)	442.33(1)	-0.0070(5)%
Shower	412.54(3)	412.56(3)	-0.004(2)%
Difference	-6.741(7)%	-6.730(7)%	0.003(2)%

Table 4: Showered Results: IFI Contributions to A_{FB} and to A_4

A_{FB}	No IFI (pb)	With IFI (pb)	Difference
No Shower	0.01129(2)	0.01132(2)	$(2.9 \pm 1.1) \times 10^{-5}$
Shower	0.01235(5)	0.01241(5)	$(5.8 \pm 2.6) \times 10^{-5}$
Difference	0.00106(5)	0.00109(5)	$(2.9 \pm 2.8) \times 10^{-5}$
A_4	No IFI (pb)	With IFI (pb)	Difference
No Shower	0.06057(3)	0.06102(3)	$(4.5 \pm 0.3) \times 10^{-4}$
Shower	0.06003(8)	0.06052(8)	$(4.9 \pm 0.8) \times 10^{-4}$
Difference	-0.00055(8)	-0.00050(8)	$(4.3 \pm 8.5) \times 10^{-5}$

of $\sin^2 \theta_W$ from LHC data. In these studies, approaches based on collinear QED PDF's⁷ will be compared with the approach in KKMC-hh to elucidate the relationship between the different approaches with the objective of defining the relevant theoretical precision tag.

We note the ISR in $\mathcal{K}\mathcal{K}MC$ -hh is sensitive to the value of light quark masses, as discussed in Ref. [5]. The key point is that the results from Ref. [46] show that the light quark masses must be the short distance type masses with $m_u \cong 6$ MeV, $m_d \cong 10$ MeV, $m_s \cong 150$ MeV where the uncertainty may be estimated by taking the PDG [47] values $m_u = 2.2$ MeV, $m_d = 4.7$ MeV, $m_s = 96$ MeV. Since the quark masses enter via the big log $L_q = \ln(M_Z^2/m_q^2)$, we expect the fractional uncertainty in our results from such a change in our masses to be at the level of the weighted fractional change in L_q , which is $\langle \Delta L/L \rangle \cong ((\frac{4}{9}\Delta L_u + \frac{1}{9}\Delta L_d))/((\frac{4}{9}L_u + \frac{1}{9}L_d) \cong 0.10$, if use the fact that the densities of u and d quarks at the relevant momentum fractions are almost equal inside the proton. Here, $\Delta L_q = \ln(M_Z^2/m_{q2}^2) - \ln(M_Z^2/m_{q1}^2)$ for the two masses m_{qi} , $i = 1, 2$, for quark q in an obvious notation. Further studies on the role of light quark masses in EW higher order corrections in precision LHC/FCC physics are in progress and will appear elsewhere [17].

Precision studies of angular observables in single Z/γ^* production at the LHC must take the effects from EW ISR that we have discussed in this paper into account.

Acknowledgments

This work was supported in part by the Programme of the French–Polish Cooperation between IN2P3 and COPIN within the Collaborations Nos. 10-138 and 11-142 and by a grant from the Citadel Foundation. The authors also thank the IFJ-PAN, Krakow, PL for computing

⁷See Ref. [16] for a complete list of all the approaches which use collinear QED PDF's.

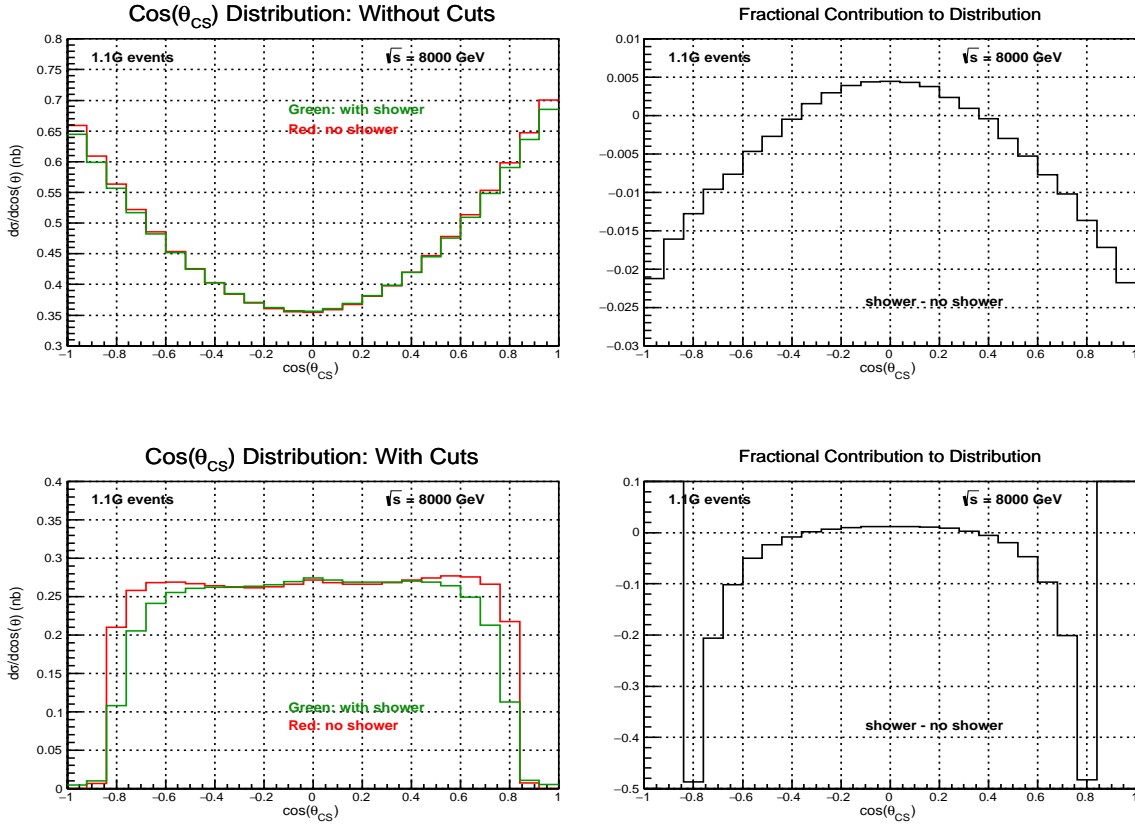


Figure 8: Showered contributions to the CS angle distribution: the two top plots are without lepton cuts (used for A_4), the two bottom plots are with lepton cuts (used for A_{FB}). Showered $\mathcal{K}\mathcal{K}MC$ -hh ISR+ FSR results are shown in green (light shade), and unshowered $\mathcal{K}\mathcal{K}MC$ -hh ISR+ FSR results are shown in red (medium dark shade). In the two plots on the right, the respective fractional contributions of the shower effects to the distributions are shown.

support and Prof. G. Giudice for the support and kind hospitality of the CERN TH Department.

References

- [1] ATLAS Collaboration, G. Aad *et al.*, *J. High Energy Phys.* **08** (2016) 159, hep-ex/1606.00689.
- [2] ATLAS Collaboration, M. Aaboud *et al.*, *Eur. Phys. J. C* **78** (2018) 110, hep-ex/1701.07240.
- [3] CDF and D0 Collaboration, T. Aaltonen *et al.*, *Phys. Rev. D* **88** (2013) 052018, hep-ex/1307.7627.
- [4] V. Abazov *et al.*, *Phys. Rev. Lett.* **106** (2011) 122001, hep-ex/1010.0262.

- [5] S. Jadach, B. F. L. Ward, Z. Wąs, and S. Yost, *Phys. Rev. D* **99** (2019) 076016, hep-ph/1707.06502.
- [6] S. Sjostrand, T. Mrenna and P. Skands, *Comput. Phys. Commun.* **178** (2008) 852, hep-ph/0710.3820.
- [7] CMS Collaboration, V. Khachatryan *et al.*, *Phys. Lett. B* **750** (2015) 154, hep-ex/1504.03512.
- [8] T. Sjostrand, “Prompt photon production in showers”, in *Workshop on Photon Radiation from Quarks* (S. Cartwright, ed.), p. 89, CERN, Geneva, 1991, CERN-92-04, Proceedings of Anecy Workshop.
- [9] S. Dittmaier, A. Huss, and C. Schwinn, *Nucl. Phys.* **B885** (2014) 318, hep-ph/1403.3216.
- [10] S. Dittmaier, A. Huss, and C. Schwinn, *Nucl. Phys.* **B904** (2016) 216, hep-ph/1511.08016.
- [11] U. Baur, S. Keller, and D. Wackerth, *Phys. Rev. D* **59** (1998) 013002, hep-ph/9807417.
- [12] U. Baur *et al.*, *Phys. Rev. D* **65** (2002) 033007, hep-ph/0108274.
- [13] S. Dittmaier and M. Kramer, *Phys. Rev. D* **65** (2002) 073007, hep-ph/0109062.
- [14] C. M. C. Calame *et al.*, *J. High Energy Phys* **0710** (2007) 109, 0911.2329.
- [15] S. Dittmaier and M. Huber, *J. High Energy Phys* **1001** (2010) 060, 0911.2329.

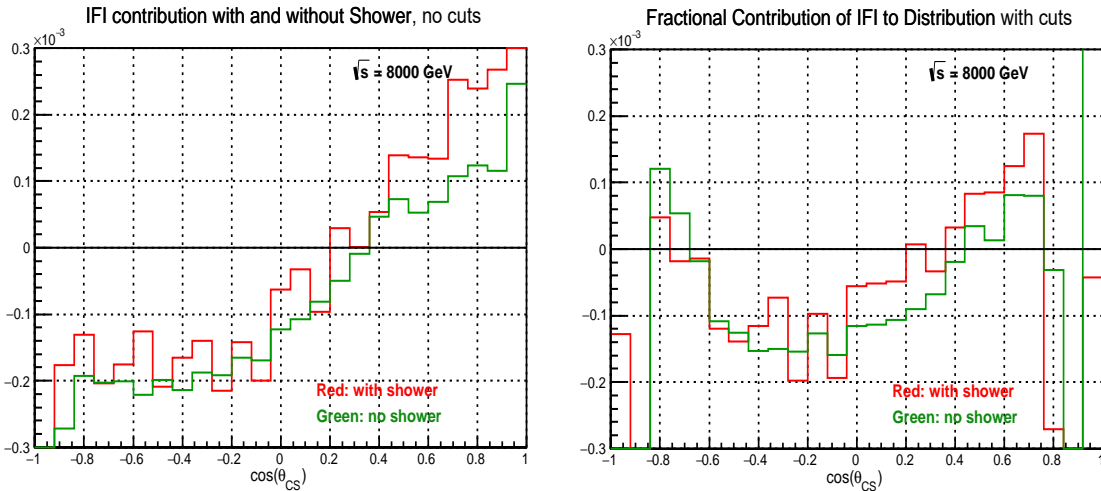


Figure 9: Dependence of the Collins-Soper angular distribution on initial-final interference, without lepton cuts (left) and with them (right). Unshowered results are shown in green (light shade), and showered results are shown in red (medium dark shade).

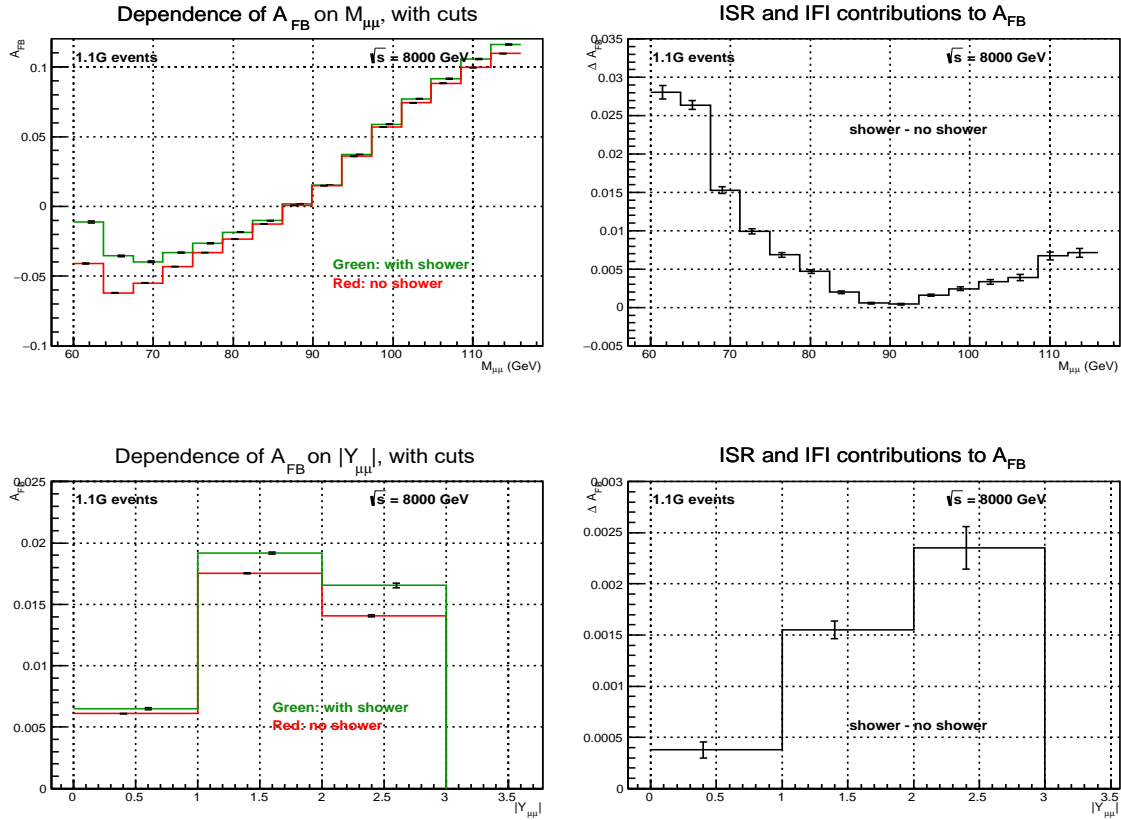


Figure 10: Showered contributions to A_{FB} : the two top plots show the shower effects as a function of $M_{\ell\ell}$, the two bottom plots show the shower effects as a function of $Y_{\ell\ell}$. Showered $\mathcal{K}\mathcal{K}MC$ -hh ISR+FSR+IFI results are shown in green (light shade), and unshowered $\mathcal{K}\mathcal{K}MC$ -hh ISR+FSR+IFI results are shown in red (medium dark shade). In the two plots on the right, the respective differences between the showered and unshowered distributions are shown.

- [16] S. Alioli *et al.*, *CERN-TH-2016-137*; *CERN-LPCC-2016-002* (2016) hep-ph/1606.02330.
- [17] S. Jadach *et al.*, to appear.
- [18] D. Froidevaux, private communication, 2019.
- [19] G. Corcella, I. G. Knowles, G. Marchesini, S. Moretti, K. Odagiri, P. Richardson, M. H. Seymour, and B. R. Webber, *JHEP* **0101** (2001) 010, hep-ph/0011363.
- [20] T. Sjostrand *et al.*, *Comput. Phys. Commun.* **135** (2001) 238.
- [21] M. Bahr *et al.*, *Eur. Phys. J. C* **58** (2008) 639, hep-ph/0803.0883.
- [22] T. Gleisberg *et al.*, *J. High Energy Phys.* **02** (2009) 007, hep-ph/0811.4622.
- [23] D. R. Yennie, S. Frautschi, and H. Suura, *Ann. Phys. (NY)* **13** (1961) 379 – 452.

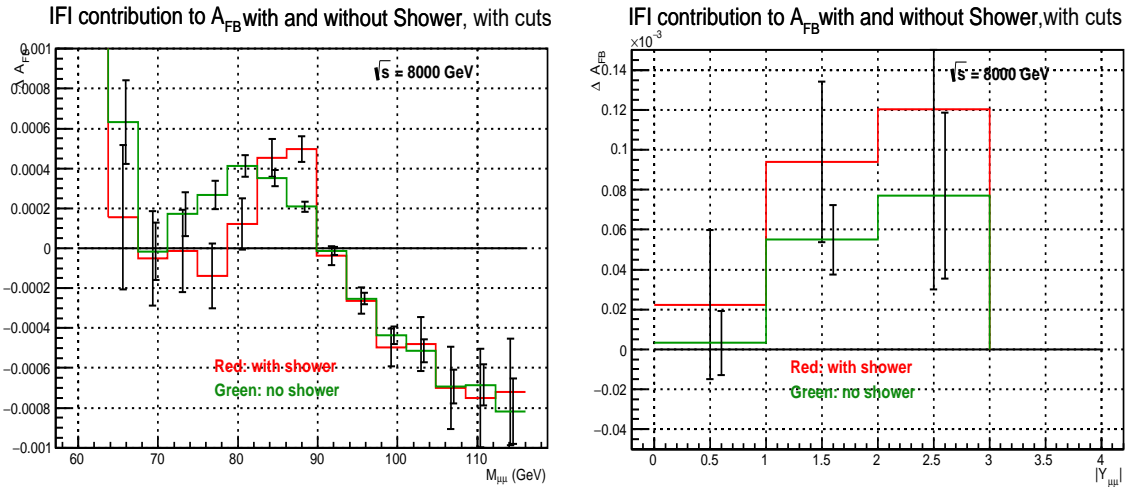


Figure 11: Shower effects on the IFI contribution to A_{FB} : the plots on the left illustrate the shower effects as a function of $M_{\ell\ell}$, the plots on the right illustrate the shower effects as a function of $Y_{\ell\ell}$. The results show the showered and unshowered differences between $\mathcal{K}\mathcal{K}MC$ -hh ISR+FSR+IFI results and the corresponding $\mathcal{K}\mathcal{K}MC$ -hh ISR+FSR results. The unshowered results are in green (light shade), the showered results are in red (medium dark shade).

- [24] F. Krauss *et al.*, *Eur.Phys. J. C* **79** (2019) 143, hep-ph/1809.10650.
- [25] B. Biedermann *et al.*, *Eur.Phys. J.* **77** (2017) 492, hep-ph/1704.05783.
- [26] S. Actis *et al.*, *Comput. Phys. Commun.* **214** (2017) 140, hep-ph/1605.01090.
- [27] S. Kallweit *et al.*, *J. High Energy Phys.* **04** (2016) 021, hep-ph/1511.0692.
- [28] S. Alioli, P. Nason, O. Oleari, and E. Re, *J. High Energy Phys.* **06** (2010) 043, hep-ph/1002.2581.
- [29] A. Arbuzov *et al.*, *Eur. Phys. J. C* **54** (2008) 451, hep-ph/0711.0625.
- [30] Y. Li and Petriello, *Phys. Rev. D* **86** (2012) 094034, hep-ph/1208.5967.
- [31] M. Delto *et al.*, *JHEP.* **01** (2020) 043, hep-ph/1909.08428.
- [32] M. Bonciani *et al.*, *Phys. Rev. D* **101** (2020) 031301, hep-ph/1911.06200.
- [33] S. Jadach, B. F. L. Ward, and Z. Was, *Comput. Phys. Commun.* **79** (1994) 503–522.
- [34] S. Jadach, B. F. L. Ward, and Z. Was, *Comput. Phys. Commun.* **130** (2000) 260–325, hep-ph/9912214.
- [35] S. Jadach, B. F. L. Ward, and Z. Was, *Phys. Rev.* **D63** (2001) 113009, hep-ph/0006359.
- [36] S. Jadach, B. F. L. Ward, and Z. Was, *Phys. Rev.* **D88** (2013), no. 11 114022, 1307.4037.

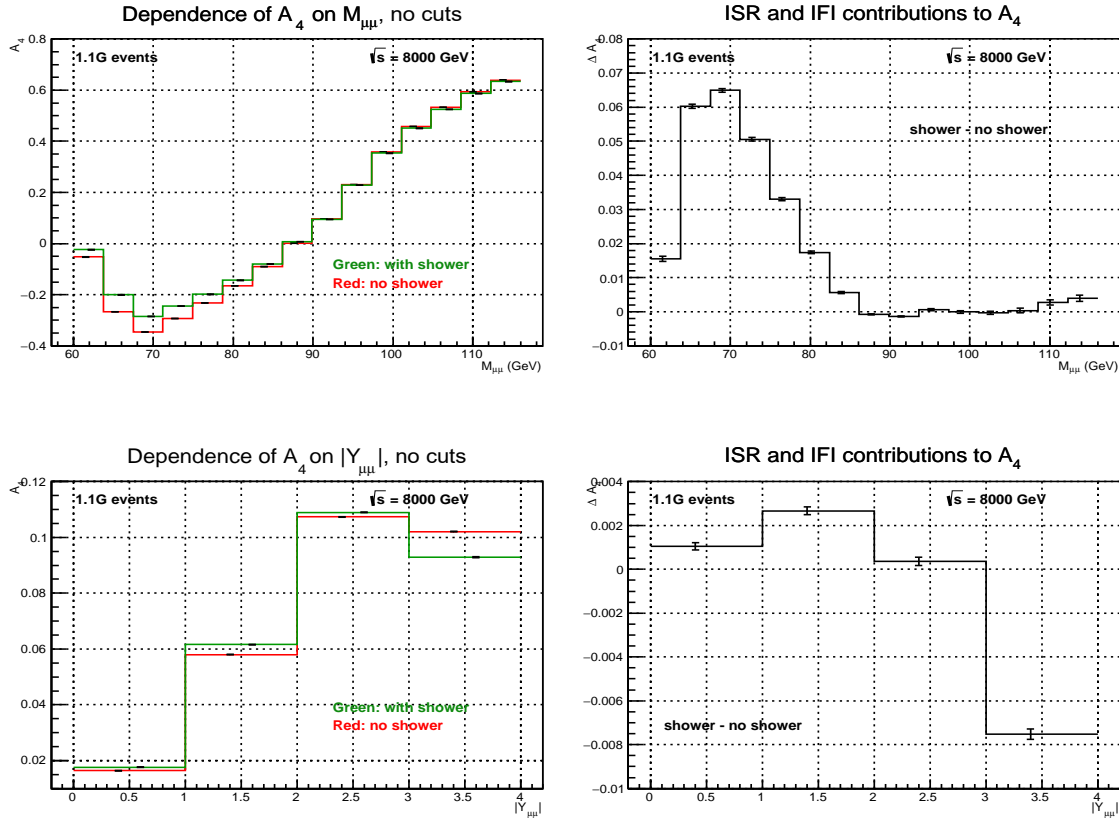


Figure 12: Showered contributions to A_4 : the two top plots show the shower effects as a function of $M_{\ell\ell}$, the two bottom plots show the shower effects as a function of $Y_{\ell\ell}$. Showered $\mathcal{K}\mathcal{K}MC$ -hh ISR+FSR+IFI results are shown in green (light shade), and unshowered $\mathcal{K}\mathcal{K}MC$ -hh ISR+FSR+IFI results are shown in red (medium dark shade). In the two plots on the right, the respective differences between the showered and unshowered distributions are shown.

[37] T. Sjostrand, *Phys. Lett.* **157B** (1985) 321.

[38] E. Boos *et al.*, hep-ph/0109068.

[39] S. Weinberg, *Phys. Rev. Lett.* **19** (1967) 1264–1266.

[40] S. L. Glashow, J. Iliopoulos, and L. Maiani, *Phys. Rev.* **D2** (1970) 1285–1292.

[41] S. L. Glashow, *Nucl. Phys.* **22** (1961) 579–588.

[42] A. Salam, *Elementary Particle Theory*. N. Svartholm (Almqvist and Wiksell), Stockholm, 1968.

[43] S. Jadach, B. F. L. Ward, Z. Was, and S. Yost, *Phys. Rev. D* **94** (2016) 074006, hep-ph/1608.01260.

[44] D. Bardin *et al.*, EW Library.

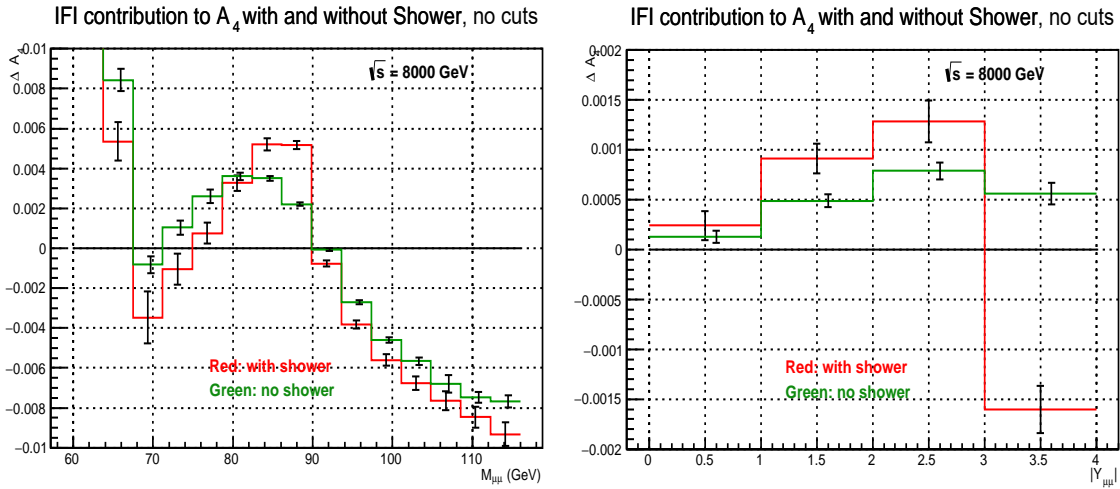


Figure 13: Shower effects on the IFI contribution to A_4 : the plots on the left illustrate the shower effects as a function of $M_{\ell\ell}$, the plots on the right illustrate the shower effects as a function of $Y_{\ell\ell}$. The results show the showered and unshowered differences between $\mathcal{K}\mathcal{K}MC$ -hh ISR+FSR+IFI results and the corresponding $\mathcal{K}\mathcal{K}MC$ -hh ISR+FSR results. The unshowered results are in green (light shade), the showered results are in red (medium dark shade).

- [45] D. Bardin *et al.*, e-print: hep-ph/9908433.
- [46] A. D. Martin *et al.*, *Eur. Phys. J. C* **39** (2005) 155, hep-ph/0411040.
- [47] Particle Data Group Collaboration, C. Patrignani *et al.*, *Chin. Phys. C* **40** (2016) 100001.
- [48] J. C. Collins and D. E. Soper, *Phys. Rev. D* **16** (1977) 2219.
- [49] ATLAS Collaboration Collaboration, G. Aad *et al.*, *Phys. Rev. D* **85** (2012) 072004, 1109.5141.
- [50] E. Mirkes, *Nucl. Phys. B* **387** (1992) 3–85.
- [51] A. Manohar, P. Nason, G. P. Salam, and G. Zanderighi, *Phys. Rev. Lett.* **117** (2016) 242002.
- [52] R. D. Ball *et al.*, 1706.00428.